Available online at www.sciencedirect.com
ScienceDirect
Trans. Nonferrous Met. Soc. China 31(2021) 666−678
Transactions of Nonferrous Metals Society of China
www.tnmsc.cn

Fabrication of fine-grained, high strength and toughness Mg alloy by extrusion−shearing process

Bo-ning WANG[1,2], Feng WANG[1,2], Zhi WANG[1,2], Zheng LIU[1,2], Ping-li MAO[1,2]

1. School of Materials Science and Engineering, Shenyang University of Technology, Shenyang 110870, China;
2. Key Laboratory of Magnesium Alloys and Processing Technology of Liaoning Province, Shenyang 110870, China

Received 5 May 2020; accepted 20 October 2020

Abstract: A novel extrusion−shearing (ES) composite process was designed to fabricate fine-grained, high strength and tough magnesium alloy. The structural parameters of an ES die were optimized by conducting an orthogonal simulation experiment using finite element software Deform-3D, and Mg−3Zn−0.6Ca−0.6Zr (ZXK310) alloy was processed using the ES die. The results show that the optimized structural parameters of ES die are extrusion angle (α) of 90°, extrusion section height (h) of 15 mm and inner fillet radius (r) of 10 mm. After ES at an extrusion temperature and a die temperature of 350 °C, ZXK310 alloy exhibited good ES forming ability, and obvious dynamic recrystallization occurred in the forming area. The grain size decreased from 1.42 μm of extrusion area to 0.85 μm of the forming area. Owing to the pinning of second phase and formation of ultrafine grains, the tensile strength, yield strength and elongation of alloy reached 362 MPa, 289 MPa and 21.7%, respectively.

Key words: Mg−Zn−Ca−Zr alloy; extrusion−shearing process; die design; dynamic recrystallization; mechanical properties

1 Introduction

Magnesium (Mg) alloys are promising lightweight materials for engineering applications owing to their low density, high specific strength and good shock absorption [1−3]. However, the insufficient strength and toughness of conventional Mg alloys hinder their widespread utilization. According to the Hall−Petch (H−P) relationship, grain refinement is an effective method to improve the strength of different materials, and the strength increases with decreasing grain size [4].

The most significant method for the grain refinement of Mg alloys is severe plastic deformation (SPD). For instance, HUANG et al [5] prepared high-performance Mg alloys using equal channel angular pressing (ECAP); the ultimate tensile strength of ECAP alloy reached 372 MPa due to fine DRX particles, ultrafine second phase, and nanoprecipitates. HORKY et al [6] used high-pressure torsion (HPT) to obtain Mg alloys with submicron grain size. Moreover, WANG et al [7] and TROJANOVÁ et al [8] prepared fine-grained superplastic Mg alloys by accumulative roll bonding (ARB). These results show that the grain structure of Mg alloys can be effectively refined by SPD, leading to superior mechanical properties. In addition, some unconventional SPD methods have been reported to avoid repeated multiple processes. HU et al [9] combined two-part ECAP die to achieve SPD through consecutive shears and obtained ultrafine-grained Mg alloys. BAGHERPOUR et al [10] prepared ultrafine-grained copper (Cu) through a multipass simple shear extrusion (SSE) process. BISADI et al [11]

Corresponding author: Feng WANG; Tel: +86-15002424621; Fax: +86-24-25496301; E-mail: wf9709@126.com
DOI: 10.1016/S1003-6326(21)65528-0
1003-6326/© 2021 The Nonferrous Metals Society of China. Published by Elsevier Ltd & Science Press

combined ECAP and twist extrusion (TE) to develop a symmetrical channel angular pressing (SCAP) process; the results showed that compared with ECAP, the SCAP alloy exhibited high performance and more uniform strain. Notably, the conventional SPD process, i.e., HPT, cannot be used to prepare large-sized samples, whereas the ARB process is promising for large-scale applications due to its convenient equipment. However, the utilization of ARB increases the number of interfaces of the plate when it is stacked. Consequently, poor interfacial bonding leads to inferior mechanical properties. Compared with HPT and ARB, ECAP renders superior grain refinement and easy implementation without altering the cross-sectional size [12].

During ECAP, the degree of grain refinement depends on the strain path, cumulative strain, processing temperature, and extrusion speed [13]. However, the alloy needs to pass through multiple extrusion cycles from an equal channel die to obtain a fine-grained structure. At present, wrought Mg alloys are mainly fabricated by conventional extrusion and ECAP methods. The conventional extrusion process is widely used to prepare fine-grained alloys with high strength, such as ZK60+1.5Nd [14] and ZK60+1.5Ce [15]. Similarly, ultrafine-grained ZK60 [16] and Mg−Gd−Nd−Zn−Zr [17] alloys were prepared by ECAP, exhibiting high strength and superior toughness. Although the grain is significantly refined by ECAP multiple deforming, these studies reveal that the effect of texture weakening is greater than the grain refinement strengthening due to continuous weakening of texture [18−20]. Finally, the yield strength of alloy decreases due to the weakening of texture, and the grain size is lower than the critical value. In addition, the die structure of ECAP also affects the mechanical properties and micro-structure of Mg alloys. Notably, the strain in ECAP is affected by the main structural parameters of die, such as channel angle and transition fillet radius. The channel angle mainly affects the magnitude of equivalent strain and in turn the degree of grain refinement. NAKASHIMA et al [21] studied the effect of channel angle (90°−157.5°) on the grain refinement of ECAP-processed pure Al. At a channel angle of 90°, pure Al sample experienced a large plastic deformation, resulting in ultrafine equiaxed crystals with large-angle grain boundaries. Recently, several studies were focused on the effect of outer fillet radius of channel angle; however, the effect of inner fillet radius on grain and strain in the shear area has not been explored yet. BALASUNDAR et al [22] systematically evaluated the ECAP die structure and showed that the inner fillet is helpful for processing materials with a high flow softening rate and improving the alloy formability. However, the equivalent strain decreased with the increase in inner fillet radius [23,24]. Hence，it is very important to design a proper die structure.

Herein, a novel extrusion−shearing (ES) process is proposed by combining the initial forward extrusion process with ECAP. Moreover, an ES die was designed and developed by combining orthogonal experiments with Deform software simulations. Moreover, Mg−3Zn−0.6Ca−0.6Zr alloy bars were processed by ES, and the effect of ES die on microstructure, textural evolution, and mechanical properties was systematically studied.

2 Experimental

The main parameters of finite element analysis (FEA) and ES simulations are given in Table 1. First, a finite element geometric model was established using a UG three-dimensional (3D) modeling software, i.e., workpiece models, cavity die, cushion block, and die sleeve (Fig. 1(a)) and saved in .STL format. The cushion block and die were defined as rigid bodies during preprocessing into Deform-3D and the workpiece was defined as a

Table 1 Main parameters of FEA and ES simulations

Parameter	Value
Extrusion temperature/°C	350
Extrusion ratio	12.25
Extrusion speed/(mm·s^{-1})	1
Billet diameter/mm	70
Friction coefficient	0.3
Billet preheating temperature/°C	350
Die preheating temperature/°C	350
Channel angular/(°)	90
Outer fillet radius of shear area, R/mm	10
Extrusion area and forming area diameter, d/mm	20

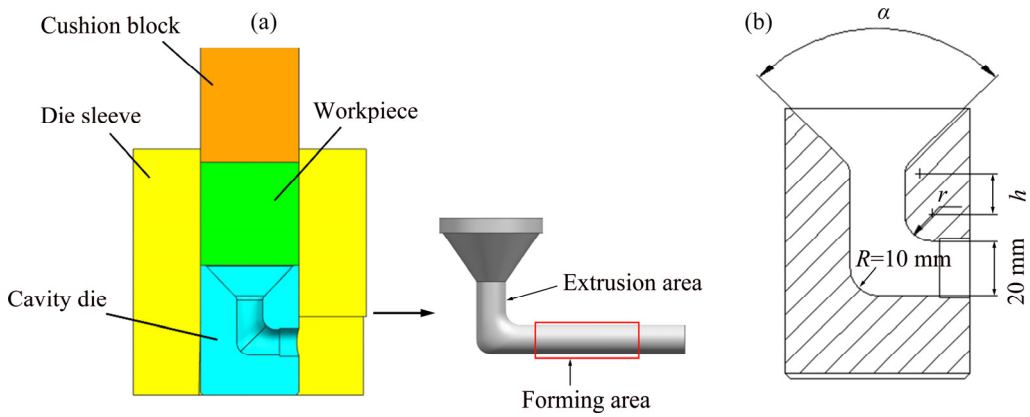

Fig. 1 Schematic illustration of die assembly model (a) and die size optimization (b)

plastic object. Moreover, the effect of die structure parameters on the forming of Mg alloy was studied to perfectly merge both the forming processes. Based on the extrusion force, equivalent strain, and equivalent stress in Deform-3D simulations, the orthogonal method was used to design and optimize the die structural parameters, i.e., die extrusion angle (α), extrusion section height (h), and fillet radius (r) in the shear area, as shown in Fig. 1(a). Also, the size optimization diagram of the die is shown in Fig. 1(b). Then, the initial forward extrusion and ECAP were combined to achieve fine-grained structure, with high strength and toughness. Therefore, the designed die was mainly composed of four parts: necking area, extrusion area, shearing area, and forming area. Notably, the shearing effect can be achieved after extrusion by using ES die. This continuously generates dynamic recrystallization, leads to deformation strengthening, refines the grain structure, and enhances the mechanical properties. In addition, the proposed ES model also provides an idea to adjust the extrusion ratio by optimizing the diameter of workpiece and bar diameter of forming area. Moreover, a large extrusion ratio (>50%) can be obtained by multiple ES, which is highly desirable for SPD.

Moreover, Mg−3Zn−0.6Ca−0.6Zr (ZXK310) alloy ingots were prepared using high-purity (99.95%) Mg, Zn and Mg−20Ca (wt.%), and Mg−30Zr (wt.%) raw materials. Briefly, pure Mg was melted at 700 °C by using a resistance furnace under the protection of 99.5 vol.% N_2 and 0.5 vol.% SF_6. Then, Zn, Mg−20Ca (wt.%), and Mg−30Zr (wt.%) were added into the melt, and the temperature was increased to 720 °C. The temperature was maintained at 720 °C for 30 min to ensure that alloying elements are homogeneously dissolved. Subsequently, the temperature was lowered to 700 °C, and the melt was poured into a metallic mold (d75 mm × 75 mm), which was coated with boron nitride (BN) and preheated at 200 °C. The cylindrical specimens (d70 mm × 70 mm) were sectioned and homogenized at 380 °C for 18 h. Then, an ES experiment was carried out at 350 °C. In addition, the microstructure was analyzed using a JEM−2100 transmission electron microscope (TEM) operating at 200 kV. Electron backscattered diffraction (EBSD) analysis was conducted on a Gemini SEM 300 equipped with an HKL-EBSD system operating at 15 kV with a step size of 0.2 μm. For TEM imaging, circular flakes with thickness of 45 μm and diameter of 3 mm were prepared using metallographic method. Subsequently, the circular sheet sample was placed in a 3.5 kV Gatan 691 ion beam of 4° until a pinhole appeared near the center. For EBSD imaging, circular flakes with thickness of 45 μm and diameter of 3 mm were prepared using metallographic method. Subsequently, the circular sheet sample was placed in a 5 kV Gatan 691 ion beam of 4° for 1 h. Tensile samples with a gauge length of 10 mm and a thickness of 2 mm were obtained from the forming area in the ES bar using an electric spark machine. Tensile tests were performed at ambient temperature using a WDW−100 universal testing machine at an initial strain rate of 1×10^{-3} s^{-1} with load direction parallel to extrusion direction (ED).

3 Results and discussion

3.1 Design and optimization of structural parameters

Table 2 shows the factors−levels of orthogonal

Table 2 Factors−levels of orthogonal test for die structural parameters

Level	Factor		
	α(A)/(°)	h(B)/mm	r(C)/mm
1	60	15	5
2	90	20	10
3	120	25	15

test for die structural parameters. The die structural parameters consist of three factors, including the extrusion angle (α), height (h) of the extrusion section, and inner fillet radius (r) of shear area. Nine groups of geometric models were established using the test parameters, as shown in Fig. 2.

The extrusion force, equivalent strain, and equivalent stress in the stable extrusion stage were selected to study the effect of die parameters on ES forming. During ES, the extrusion force reflects the difficulty of forming and sets requirements for die strength and press machine. The equivalent strain reflects the degree of deformation and the effect of grain refinement. The equivalent stress indicates the difficulty and failure of bar forming, i.e., larger equivalent stress hinders the forming and facilitates failure.

Then, nine groups of ES geometric models were imported into Deform-3D software to simulate the extrusion. The orthogonal test results are given in Table 3. The extreme difference (R*) indicates the primary- and secondary-order of effect of die structural parameters. In the case of extrusion force, the primary- and secondary-order of effect follows the given order: extrusion angle (α), extrusion

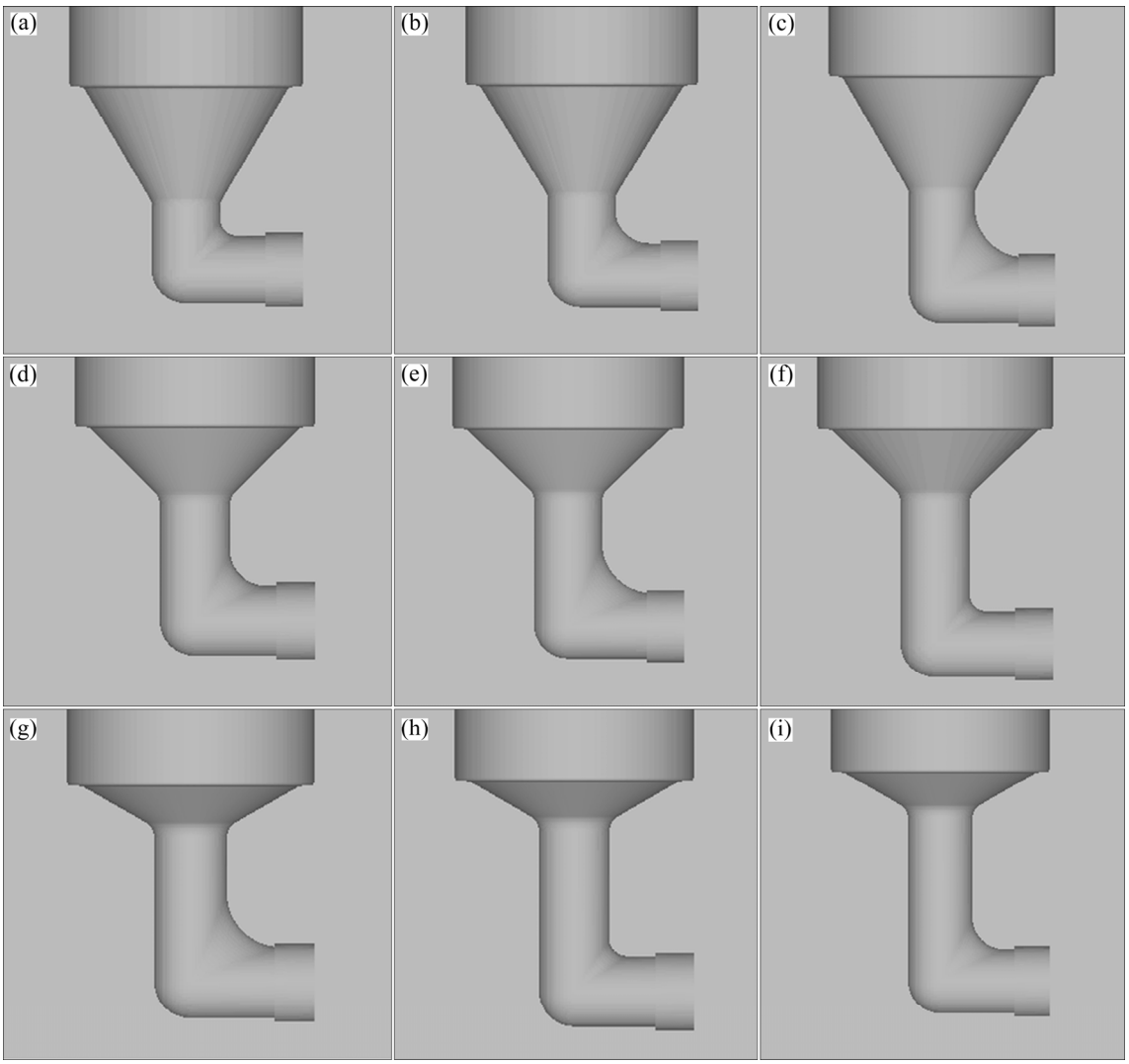

Fig. 2 3D geometric models with different structural parameters: (a) α=60°, h=15 mm, r=5 mm; (b) α=60°, h=20 mm, r=10 mm; (c) α=60°, h=25 mm, r=15 mm; (d) α=90°, h=15 mm, r=10 mm; (e) α=90°, h=20 mm, r=10 mm; (f) α=90°, h=25 mm, r=5 mm; (g) α=120°, h=15 mm, r=15 mm; (h) α=120°, h=20 mm, r=5 mm; (i) α=120°, h=25 mm, r=10 mm

Table 3 Orthogonal test results

Test No.	α(A)/(°)	h(B)/mm	r(C)/mm	Load/kN	Strain	Stress/MPa
1	1	1	1	1234	8.7	49.2
2	1	2	2	1260	4.9	50.7
3	1	3	3	1332	6.4	44.0
4	2	1	2	1144	6.9	46.5
5	2	2	3	1338	8.5	48.6
6	2	3	1	1218	8.4	47.0
7	3	1	3	1314	6.1	41.8
8	3	2	1	1330	3.6	37.4
9	3	3	2	1406	5.3	49.3
k1(Load)	1271	1231	1261	Optimal combination: A2B1C1		
k2 (Load)	1232	1309	1270			
k3 (Load)	1356	1335	1288			
R* (Load)	124	104	27			
k1 (Strain)	6.7	7.2	6.9	Optimal combination: A2B1C2		
k2 (Strain)	7.9	6.1	6.9			
k3 (Strain)	5.0	6.7	5.7			
R* (Strain)	2.9	1.1	1.2			
k1 (Stress)	47.9	45.8	45.1	Optimal combination: A3B2C3		
k2 (Stress)	47.4	45.5	48.8			
k3 (Stress)	42.8	45.7	44.3			
R* (Stress)	5.1	0.3	4.5			

section height (h), and radius of inner fillet in the shear area (r). On the other hand, the primary- and secondary-order of influence on equivalent strain and equivalent stress follows the order: extrusion angle (α), radius of inner fillet in shear area (r), and extrusion section height (h). Hence, a molding method with small extrusion force, large equivalent strain, and small equivalent stress should be selected to extrude a smooth billet. The optimal combination was found to be A2, B1 and C2, corresponding to an extrusion angle (α) of 90°, extrusion section height (h) of 15 mm, and inner fillet radius (r) of 10 mm.

3.2 Evolution of equivalent strain during ES

Figure 3 shows the distribution of internal equivalent strain during ES deformation. Unlike conventional extrusion, the ES process exhibited four distinct stages of extrusion. First, the necking stage appeared with a small deformation and a small strain of 0.35 was generated at the contact point of die cone angle (Fig. 3(a)). Second, the extrusion cushion block continued to press down and the billet started to produce plastic deformation during the extrusion stage. Consequently, the strain increased from 1.73 to 2.42 from the cup-shaped region to the extrusion area. Moreover, the extrusion force overcame the deformation resistance inside the billet and friction force among the billets, die, and die sleeve; dynamic recrystallization occurred when the deformation was greater than the critical deformation. Third, the extrusion cushion block continued to push down during the shearing stage and resulted in a maximum billet strain of 3.56 after passing through a 90° corner (Fig. 3(b)). Fourth, the extrusion cushion block continued to press down and the strain gradually decreased after passing through the corner during the forming stage. Finally, the billet was stably extruded.

Notably, the ES introduced compression and shearing strain into the alloy. Herein, the extrusion

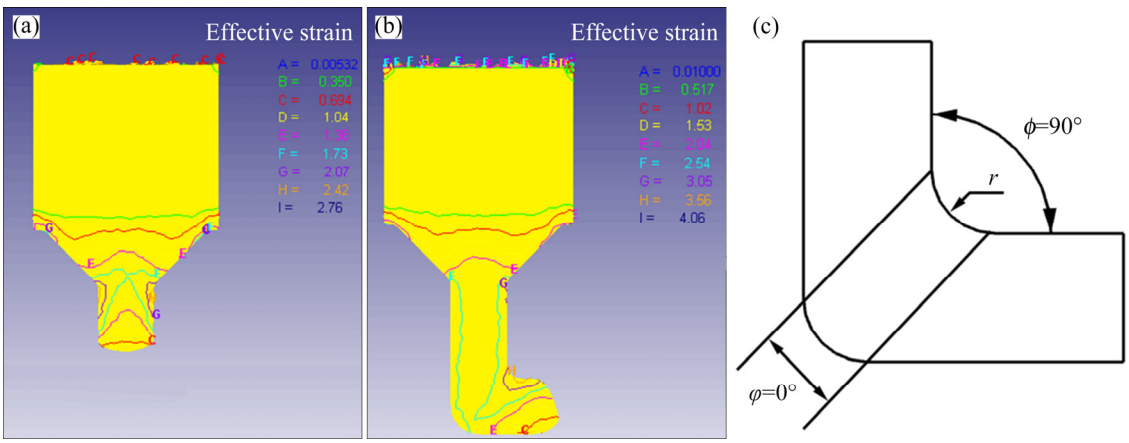

Fig. 3 Equivalent strain distribution (a, b) and shear area diagram (c) during ES deformation

ratio is 12.25, and the initial two stages of ES process are ordinary extrusion processes. The simulation results show that the maximum strain during the first and second stages is 2.42. Also, the average strain is 2.505 during the extrusion stage (Eq. (1)). SEGAL [25] utilized ECAP to obtain pure shear deformation and Eq. (2) to estimate the average strain during ECAP. It is assumed that the specimen is subjected to uniform shear deformation during ECAP, which does not exist in the actual situation. In addition, there is a radius of inner fillet angle in the channel angle of designed die in this study, where the channel angle (ϕ) is 90°, and the outer angle (φ) is 0°, as shown in Fig. 3(c). There is also a certain bending deformation during the mold shear deformation. Hence, the estimation of equivalent strain becomes complex and the average strain for the given die structure cannot be calculated from SEGAL's equation. However, the existence of inner fillet radius extends the lifetime of die, improves the surface quality of workpiece, and enhances the grain uniformity by reducing strain concentration [26]. In addition, the strain concentration at the corner of die channel causes grain inhomogeneity and the corner gaps [27] lead to nonuniform deformation during ECAP. Hence, the radius of inner fillet plays an important role in relieving strain concentration and improving alloy forming quality. The shearing area simulation results show that the strains at the outer and inner corners of shearing area are 2.54 and 3.56, respectively. Moreover, LUIS PÉREZ [28] proposed an equivalent strain calculation equation, including the radius of inner fillet angle (Eq. (3)). Therefore, the cumulative strain of ES die, expressed using Eqs. (1) and (3), was found to be 3.66:

$$\varepsilon_1=\ln\lambda \tag{1}$$

$$\varepsilon_2=1/\sqrt{3}\left[2\cot\left(\frac{\varphi}{2}+\frac{\phi}{2}\right)\right]+\phi\csc\left(\frac{\varphi}{2}+\frac{\phi}{2}\right) \tag{2}$$

$$\varepsilon_3=2/\sqrt{3}\cot\frac{\varphi}{2} \tag{3}$$

where ε is the strain, λ is the extrusion ratio. Figure 4(a) shows the physical diagram of extrusion−shear die, based on the structural parameters and simulation results. Moreover, Figs. 4(b, c) show the as-prepared ES alloy.

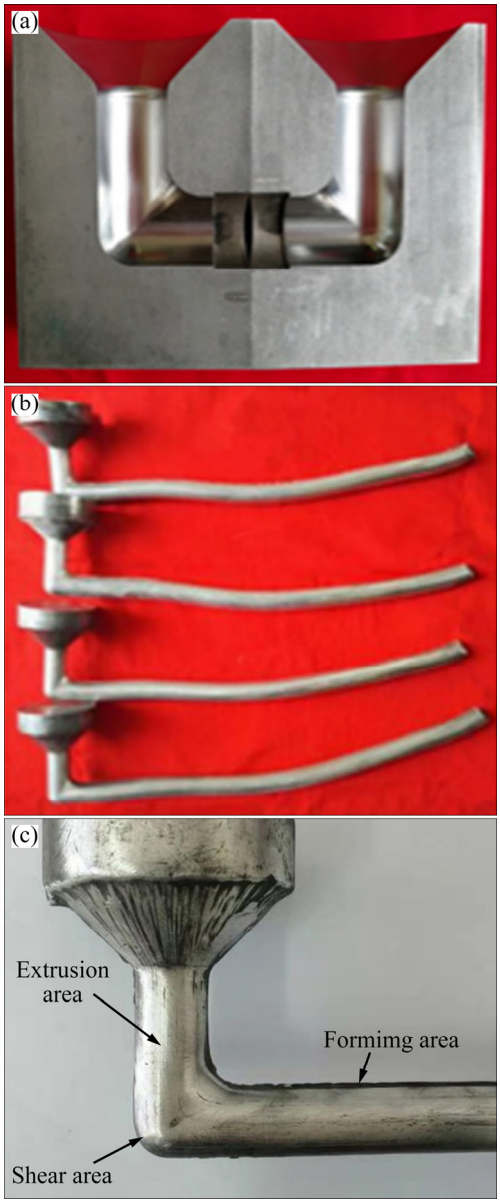

Fig. 4 Digital photograph of die (a) and ES alloy specimens (b, c)

In addition, the premise of the dynamic recrystallization of magnesium alloy during plastic deformation is that the strain must reach the critical strain of dynamic recrystallization at a certain temperature. HUANG et al [29] studied the initial DRX critical condition of AZ31 magnesium alloy. When the temperature is 573 K and the strain rate is 0.001 s^{-1}, the critical strain is 0.075, and the critical strain decreases with the increase in temperature. Therefore, DRX can occur when the extrusion temperature is 623 K (350 °C) and the strain rate is 0.001 s^{-1}. Figure 3(a) also shows that the strain of alloy reached 0.350 when it first entered the necking stage.

3.3 Microstructural characteristics and texture evolution of ES alloys

The EBSD (electron backscattered diffraction) results of extrusion and forming areas, perpendicular to ED, in extrusion−shearing ZXK310 alloy are shown in Figs. 5(a, b), showing the effect of ES on microstructural and textural evolution. The grain orientation maps indicate that the grains in the extrusion and forming areas were significantly refined, showing a bimodal structure with dynamically recrystallized (DRX) fine grains and nondynamically recrystallized (unDRX) coarse grains. Moreover, the grains were deformed, twisted, stretched, crushed, and redistributed under the action of extrusion and shearing stress. The EBSD results show that the volume fraction of dynamic recrystallization (f^{DRX}) in the forming area was higher than that of the extrusion area, i.e., the concentration of coarse unDRX grains in the forming area was significantly reduced. The f^{DRX} can be defined as follows [30]: $f^{DRX}= S_{DRX}/(S_{DRX}+S_{unDRX})$, where S_{DRX} and S_{unDRX} are the areas of DRX and unDRX regions, respectively. Notably, the grain boundaries, with a grain orientation difference of >5°, belong to DRX grains and vice versa. In the case of ES alloy, 53.5% of the extrusion area exhibited an orientation difference of >5°, which increased to 70.1% in forming area after passing through the corner shear area. Hence, the transformation from low-angle grain boundaries (LAGBs) to high-angle grain boundaries (HAGBs) occurred during ES, indicating a further increase in dynamic recrystallization [31,32]. This confirms that the corners of the die provide additional shear force and promote DRX during ES. In addition, ES alloy exhibited a fine-grained structure in the forming area, related to the reduction in the number of coarse unDRX grains. In particular, the average grain size was reduced from 1.42 μm in the extrusion area, to 0.85 μm in the forming area. Moreover, the (0001) basal plane and $(10\bar{1}0)$ prismatic plane pole figures show that the orientation of most DRX and unDRX grains changed in the forming area. A prismatic texture around the center point was formed in the extrusion area, i.e., $(10\bar{1}0)$ prismatic plane became perpendicular to ED and (0001) base plane became parallel to ED. After passing through the corner shearing area, the texture of forming area was formed with an angle of ~60° between (0001) basal

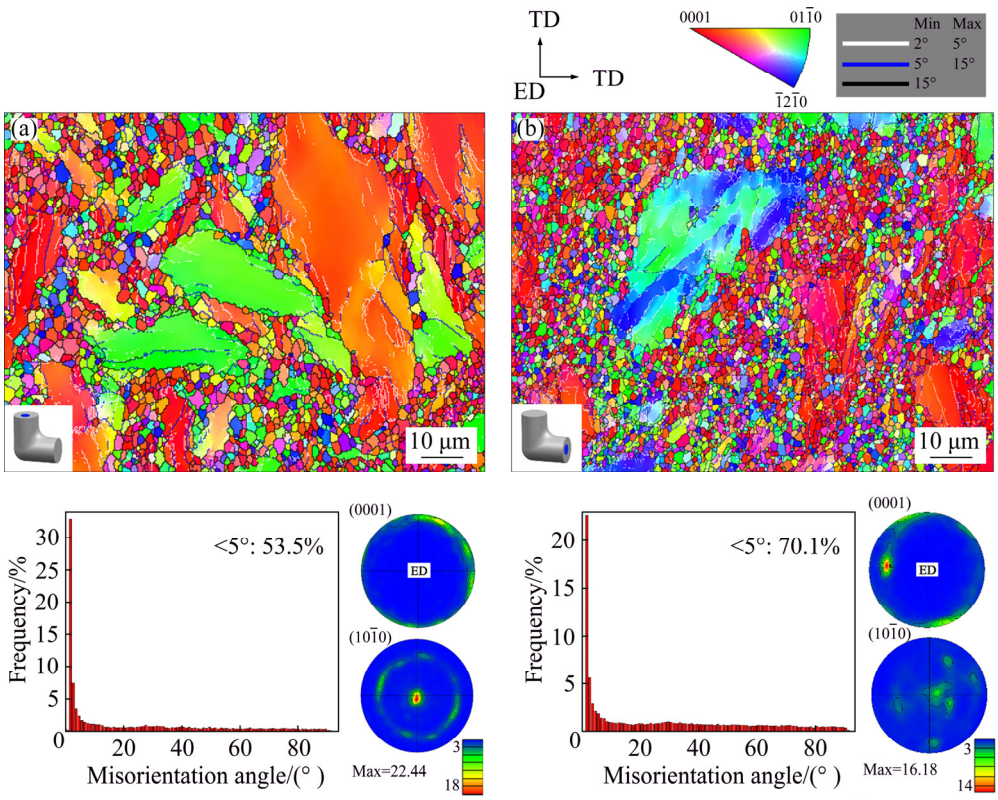

Fig. 5 EBSD orientation map, pole figure, and orientation difference distribution figures of ES ZXK310 alloy: (a) In extrusion area; (b) In forming area

plane and ED. Moreover, the prismatic plane target-type texture disappeared, and texture intensity decreased. These changes are closely related to the promotion of dynamic recrystallization due to the die corner shearing.

Furthermore, the die corner affects the microstructure, texture, and orientation of ES alloy. Herein, the unDRX and DRX regions of extrusion and forming area were analyzed using EBSD, as shown in Fig. 6. The orientation maps show that the volume fractions of nondynamic recrystallization (f^{unDRX}) in the extrusion and forming areas were 37% and 16%, respectively (Figs. 6(a, c)). Moreover, the orientation difference distribution shows that the grains in unDRX region mainly distributed with low-angle and subgrain boundaries (Figs. 6(a, c)). In addition, compared with the DRX region of extrusion area, the fraction of DRX in the forming area was obviously increased, and the grains were further refined (Figs. 6(b, d)). Moreover, the concentration of low-angle and subgrain boundaries increased in the extrusion area.

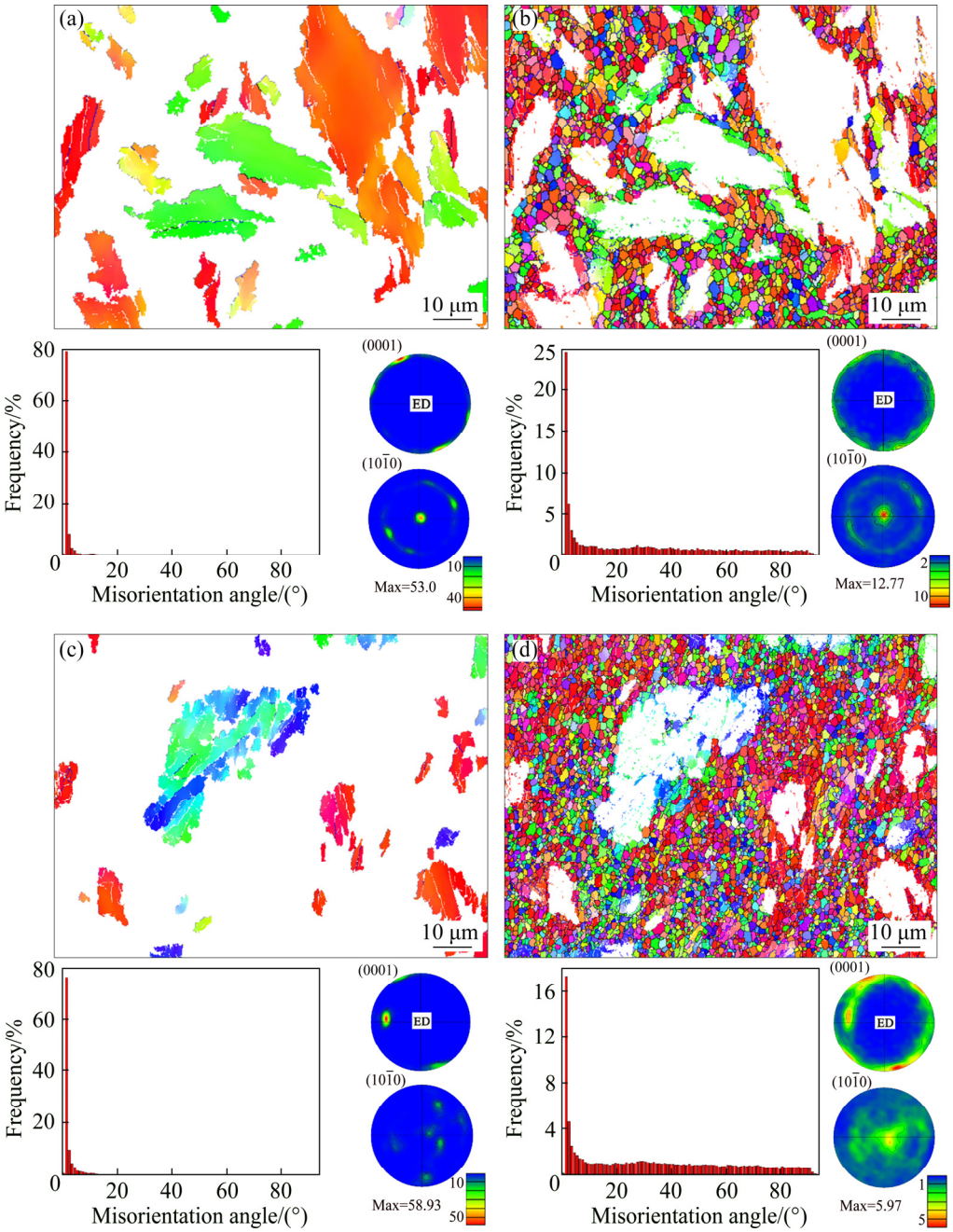

Fig. 6 EBSD results of unDRX (a, c) and DRX (b, d) regions of ES ZXK310 alloy: (a, b) In extrusion area; (c, d) In forming area

Orientation difference distributions in Figs. 6(b, d) show that a gentle micropeak transition occurred at 30° because six-fold symmetry of hexagonal structure restricted the increment of grain-to-grain orientation difference during DRX. Hence, LAGBs was observed in the unDRX region, whereas DRX grain boundaries exhibited an orientation relationship of 30°⟨0001⟩ [33]. In the unDRX region of extrusion (Fig. 6(a)) and forming areas (Fig. 6(c)), the angle between base poles and ED decreased after ES. At the same time, the texture of DRX region in the forming area weakened due to grain refinement, and the texture intensity of unDRX region in the forming area slightly increased. Hence, the additional die shearing force effectively weakened the texture and refined DRX grains [34]. Moreover, coarse unDRX grains may exist only to break larger unDRX grains into smaller unDRX grains. In general, DRX region exhibited a weaker texture and unDRX region rendered a relatively stronger texture. The textural differences between two regions affect the initiation of plastic deformation under tensile loading. Notably, the basal plane slip is initiated from the recrystallized grains due to weak basal plane texture.

The TEM image of DRX evolution of ZXK310 alloy during ES is shown in Fig. 7, perpendicular to ED. The main second phase in the alloy is $Ca_2Mg_6Zn_3$, and the corresponding diffraction spots are embedded in the TEM images. In the extrusion area, a large number of second phases accumulated at the coarse DRX grain boundaries to hinder the movement of dislocations (shown by black arrow in Fig. 7(a)). During thermal deformation, as the extrusion progressed, the subgrain boundaries continued to absorb dislocations, and the angle continued to increase. Some LAGBs became HAGBs (shown by red arrows in Fig. 7(b)). At the same time, the $Ca_2Mg_6Zn_3$ phase with a size of 200−300 nm was uniformly dispersed at the DRX grain boundaries. Figures 7(c, d) show that after passing through the corner, the alloy microstructure was obviously refined, the size of second phase became smaller and pinned at the DRX grain boundary, and a large number of HAGB appeared. The second phase distributing at the DRX grain boundaries can prevent the grain boundary migration of fine DRX grains at higher temperatures. This is conducive to obtain fine DRX grains during hot extrusion. Therefore, the formation of fine DRX grains of

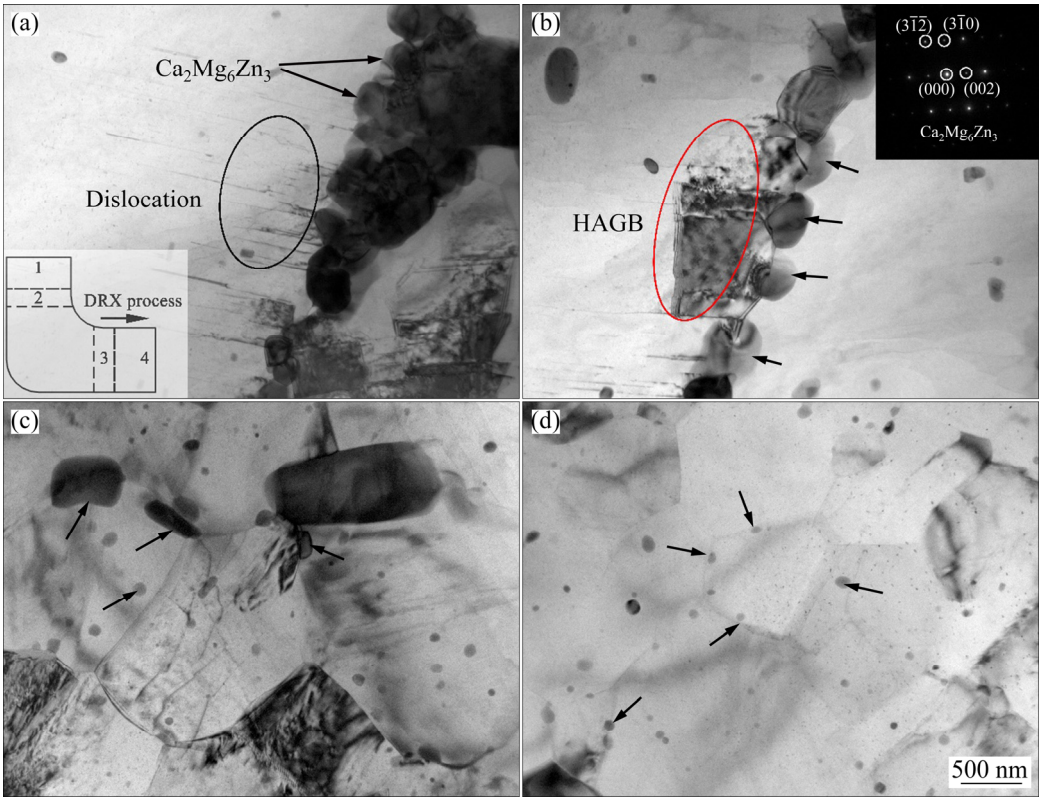

Fig. 7 Representative TEM microstructures of ES ZXK310 alloy: (a) Region 1; (b) Region 2; (c) Region 3; (d) Region 4

500−1000 nm under the pinning effect of second phase (Fig. 7(d)) is beneficial to improving the strength and toughness of ES alloy.

3.4 Microstructure and strain distribution in shearing area

Furthermore, the effect of additional shearing force on DRX and strain distribution in the die corner was evaluated. Figure 8 shows the EBSD strain distribution of shearing area of ZXK310 alloy, i.e., parallel to ED. In Regions 1, 2 and 3, the proportion of DRX, with an orientation difference angle of >5°, was 66.8%, 55.4%, and 54.6%, and the average grain size was 1.03, 1.13 and 1.12 μm, respectively. Based on the DRX grain boundaries and grain size, the DRX behavior of inner corner of the die (Region 1) is more significant than that in Regions 2 and 3. Furthermore, Fig. 8 shows that the strain gradually increased from Region 3 to Region 1, consistent with the strain variation in the corner region during Deform-3D simulations (Fig. 3). The regions with a large strain contain a high proportion of small-angle grain boundaries (white). Also, the proportion of DRX grain boundaries increased with increasing strain from the outer corner to the inner corner. The results show that the actual temperature of die shearing part significantly increased, rendering an obvious temperature gradient under the combined action of deformation heat and friction heat during extrusion shearing [35]. Notably, the large equivalent strains lead to higher temperatures in the inner corner area (Region 1). Under high-temperature and high-strain conditions, small-angle grain boundaries were annihilated, and a large number of DRX grain boundaries appeared at the inner corner area (Region 1). At the same time, a further increase in the corner temperature did not affect the grain size of forming area due to the existence of an inner fillet radius of die. Instead, the increase in corner temperature and high strain refined the grain size (0.85 μm).

3.5 Mechanical properties of ES-processed ZXK310 alloy

Figure 9 shows the tensile stress−strain curve of ES ZXK310 alloy and comparision of the mechanical properties with the Mg−Zn−Zr series wrought magnesium alloy. The ultimate tensile strength (UTS), yield strength (YS), and elongation (δ) of ES ZXK310 alloy are 362 MPa, 289 MPa, and 21.7%, respectively, demonstrating superior mechanical properties of ES ZXK310 alloy. These values are comparable to those reported for representative rare earth-containing Mg−Zn−Zr alloys, such as ZK60+1.5Ce (UTS=354 MPa and δ=19%) [15] and Mg−2Zn−0.3Zr−0.9Y (UTS=321 MPa and δ=21.9%) [36]. Compared with Mg−6Zn−0.2Ca−0.8Zr (UTS=357 MPa and δ=18%) [37], ZK60−1La (UTS=360 MPa and δ=13%) [38], ZK60+1.5Cu (UTS=342 MPa and δ=22.6%) [39], and Mg−10Zn−6Y−0.5Zr (UTS=368 MPa and δ=6.8%) [40] alloys, which contain a higher Zn content, ZXK310 simultaneously renders high plasticity and high strength. In addition, the radius of inner fillet, existing in the corner shear area of ES die, may reduce the shear strain. However, the average grain size of ES alloy reached 0.85 μm due to appropriate extrusion

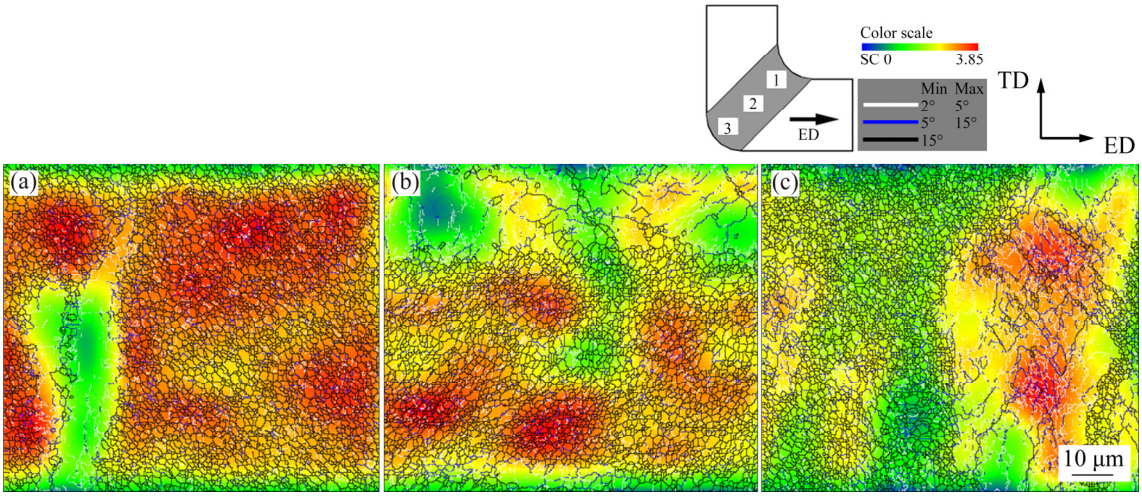

Fig. 8 EBSD strain distributions of ES ZXK310 alloy in shear area: (a) Inner corner (Region 1); (b) Central area (Region 2); (c) Outer corner (Region 3)

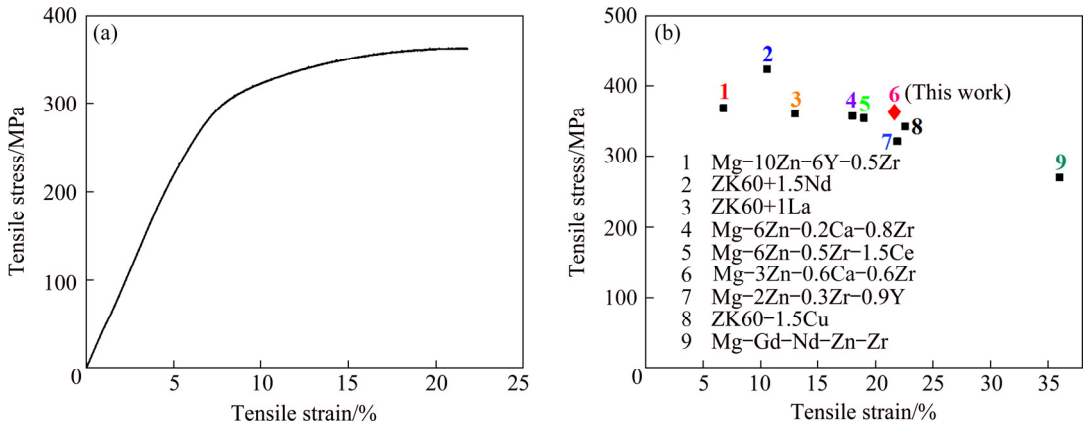

Fig. 9 Tensile stress−strain curve of ES ZXK310 alloy (a) and comparison with Mg−Zn−Zr series wrought Mg alloys (b)

Table 4 Mechanical properties of Mg−Zn−Zr series deformed alloys

Alloy	Method	Extrusion ratio	Grain size/μm	UTS/MPa	Elongation/%	Reference
ZK60+1.5Cu	Indirect extrusion	25:1	3.4	342	22.6	[39]
Mg−2Zn−0.3Zr−0.9Y	Direct extrusion	28:1	1.76	321	21.9	[36]
Mg−6Zn−0.2Ca−0.8Zr	Indirect extrusion	20:1	2	357	18	[37]
Mg−6Zn−0.5Zr−1.5Ce	Indirect extrusion	50:1	1.1	354	19	[15]
ZK60+1La	Direct extrusion	16:1	2.8	360	13	[38]
Mg−10Zn−6Y−0.5Zr	Indirect extrusion	17:1	2	368	6.8	[40]
ZK60 +1.5Nd	Direct extrusion	7:1	1.5	424	10.6	[14]
Mg−Gd−Nd−Zn−Zr	ECAP−8P	0	1.5	270	36	[17]
Mg−3Zn−0.6Ca−0.6Zr	Extrusion−shear	12.25:1	0.85	362	21.7	This work

section height and extrusion angle. Compared with the same type of Mg−Zn−Zr series alloys, the proposed die structure exhibited effective grain refinement. The mechanical properties of Mg−Zn−Zr alloys are given in Table 4. The superior strength and plasticity of ZXK310 alloy can be mainly attributed to the pinning effect of broken second DRX grains, ultrafine grains in the forming area, and deflection of base poles.

4 Conclusions

(1) Equivalent strain and higher temperature at the corner of die led to further DRX, and refined the second phase in the alloy, in turn inhibiting DRX grain growth.

(2) In the shearing region, the inner die corner exhibited a higher strain and more DRX grain boundaries than the outer corner and center area. Also, the inner die corner rendered the most refined grain structure.

(3) Furthermore, the ES significantly improved the dynamic recrystallization of forming area, weakened the texture, and refined the grain size to 0.85 μm. Owing to the deflection of base poles, second phase pinning, and formation of ultrafine grains, the ultimate tensile strength, yield strength, and elongation of ES ZXK310 alloy reached 362 MPa, 289 MPa, and 21.7%, respectively.

Acknowledgments

This work is supported by Liaoning Revitalization Talents Program, China (XLYC1807021), Joint Research Fund of Liaoning — Shenyang National Laboratory for Materials Science, China (2019JH3/30100014), Innovation Talent Program in Sciences and Technologies for Young and Middle-aged Scientists of Shenyang, China (RC200414), and Scientific Research Fund of Liaoning Provincial Department of Education, China (LJGD2020008).

References

[1] BAMBERGER M, DEHM G. Trends in the development of new Mg alloys [J]. Annual Review of Materials Research, 2008, 38: 505−533.

[2] YOU S, HUANG Y, KAINER K U, HORT N. Recent research and developments on wrought magnesium alloys [J]. Journal of Magnesium and Alloys, 2017, 5: 239−253.

[3] MORDIKE B L, EBERT T. Magnesium−properties−applications−potential [J]. Materials Science and Engineering A, 2001, 302: 37−45.

[4] YU H H, LI C E, XIN Y C, CHAPUIS A, HUANG X X, LIU Q. The mechanism for the high dependence of the Hall−Petch slope for twinning/slip on texture in Mg alloys [J]. Acta Materialia, 2017, 128: 313−326.

[5] HUANG H, LIU H, WANG C, SUN J P, BAI J, XUE F, JIANG J H, MA A B. Potential of multi-pass ECAP on improving the mechanical properties of a high-calcium-content Mg−Al−Ca−Mn alloy [J]. Journal of Magnesium and Alloys, 2019, 7: 617−627.

[6] HORKY J, GHAFFAR A, WERBACH K, MINGLER B, POGATSCHER S, SCHAUBLIN R, SETMAN D, ZEHETBAUER M J. Exceptional strengthening of biodegradable Mg−Zn−Ca alloys through high pressure torsion and subsequent heat treatment [J]. Materials, 2019, 12: 2460.

[7] WANG Q F, XIAO X P, HU J, XU W W, ZHAO X Q, ZHAO S J. An ultrafine-grained AZ31 magnesium alloy sheet with enhanced superplasticity prepared by accumulative roll bonding [J]. Journal of Iron & Steel Research International, 2007, 14: 167−172.

[8] TROJANOVÁ Z, DŽUGAN J, HALMEŠOVÁ K, NÉMETH G, MINÁRIK P, LUKÁČ P, BOHLEN J. Influence of accumulative roll bonding on the texture and tensile properties of an AZ31 magnesium alloy sheets [J]. Materials, 2018, 11: 73.

[9] HU H J, LIU Y, ZHANG D F, OU Z N. The influences of extrusion−shear process on microstructures evolution and mechanical properties of AZ31 magnesium alloy [J]. Journal of Alloys and Compounds, 2017, 695: 1088−1095.

[10] BAGHERPOUR E, QODS F, EBRAHIMI R, MIYAMOTO H. Nanostructured pure copper fabricated by simple shear extrusion (SSE): A correlation between microstructure and tensile properties[J]. Materials Science and Engineering A, 2017, 679: 465−475.

[11] BISADI H, MOHAMADI M R, MIYANAJI H, ABDOLI M. A modification on ECAP process by incorporating twist channel [J]. Journal of Materials Engineering and Performance, 2013, 22: 875−881.

[12] MINARIK P, KRAL R, ČÍŽEK J, CHMELÍK F. Effect of different *c*/*a* ratio on the microstructure and mechanical properties in magnesium alloys processed by ECAP [J]. Acta Materialia, 2016, 107: 83−95.

[13] KRAJŇÁK T, MÁTHIS K, JANEČEK M, GUBICZA J. Comparison of the microstructure and the mechanical properties of AX41 magnesium alloy processed by EX-ECAP via three different routes A, Bc and C [C]//IOP Conference Series: Materials Science and Engineering, 2014, 63: 012058.

[14] LV S H, MENG F Z, LU X L, YANG Q, QIU X, DUAN Q, MENG J. Influence of Nd addition on microstructures and mechanical properties of a hot-extruded Mg−6.0Zn−0.5Zr (wt.%) alloy [J]. Journal of Alloys and Compounds, 2019, 806: 1166−1179.

[15] JEONG H Y, KIM B, KIM S, KIM H J, PARK S S. Effect of Ce addition on the microstructure and tensile properties of extruded Mg−Zn−Zr alloys [J]. Materials Science and Engineering A, 2014, 612: 217−222.

[16] YUAN Y C, MA A, GOU X F, JIANG J H, LU F M, SONG D, ZHU Y T. Superior mechanical properties of ZK60 Mg alloy processed by equal channel angular pressing and rolling [J]. Materials Science and Engineering A, 2015, 630: 45−50.

[17] LIU Y, KANG Z X, ZHOU L L, ZHANG J Y, LI Y Y. Mechanical properties and biocorrosion behaviour of deformed Mg−Gd−Nd−Zn−Zr alloy by equal channel angular pressing [J]. Corrosion Engineering Science and Technology, 2016, 51: 256−262.

[18] KIM W J, HONG S I, KIM Y S, MIN S H, JEONG H T, LEE J D. Texture development and its effect on mechanical properties of an AZ61 Mg alloy fabricated by equal channel angular pressing [J]. Acta Materialia, 2003, 51: 3293−3307.

[19] KIM W J, AN C W, KIM Y S, HONG S I. Mechanical properties and microstructures of an AZ61 Mg alloy produced by equal channel angular pressing [J]. Scripta Materialia, 2002, 47: 39−44.

[20] AKBARIPANAH F, FERESHTEH-SANIEE F, MAHMUDI R, KIM H K. Microstructural homogeneity, texture, tensile and shear behavior of AM60 magnesium alloy produced by extrusion and equal channel angular pressing [J]. Materials & Design, 2013, 43: 31−39.

[21] NAKASHIMA K, HORITA Z, NEMOTO M, ANGDONL T G. Development of a multi-pass facility for equal-channel angular processing to high total strains [J]. Materials Science and Engineering A, 2000, 281: 82−87.

[22] BALASUNDAR I, SUDHAKARA RAO M, RAGHU T. Equal channel angular pressing die to extrude a variety of materials [J]. Materials & Design, 2009, 30: 1050−1059.

[23] HU H J, ZHANG D F, PAN F S. Die structure optimization of equal channel angular extrusion for AZ31 magnesium alloy based on finite element method [J]. Transactions of Nonferrous Metals Society of China, 2010, 20: 259−266.

[24] ZHANG X H, CHENG Y S. Influence of inner fillet radius on effective strain homogeneity in equal channel angular pressing [J]. International Journal of Advanced Manufacturing Technology, 2017, 92: 4001−4008.

[25] SEGAL V M. Equal channel angular extrusion: From macromechanics to structure formation [J]. Materials Science and Engineering A, 1999, 271: 322−333.

[26] AMINNUDIN P, PURNOWIDODO A, IRAWAN Y S, HARUYANA S, KAMINISHI K. Evaluation grain homogeneity of aluminium after ECAP process by ECAP geometry analysis using Taguchi method [J]. Key Engineering Materials, 2013, 594−595: 896−901.

[27] KARPUZ P, SIMSIR C, GUR C H. Investigating the effects of hardening of aluminium alloys on equal-channel angular pressing—A finite-element study [J]. Materials Science and

Engineering A, 2009, 503: 148−151.

[28] LUIS PÉREZ C J. On the correct selection of the channel die in ECAP processes [J]. Scripta Materialia, 2004, 50: 387−393.

[29] HUANG G, QIAN B, WANG L, JONAS J J. Study on the critical conditions for initial dynamic recrystallization of AZ31 magnesium alloy [J]. Rare Metal Materials & Engineering, 2007, 36: 2080−2083.

[30] DENG K K, WANG X J, ZHENG M Y, WU K. Dynamic recrystallization behavior during hot deformation and mechanical properties of 0.2 μm SiC_p reinforced Mg matrix composite [J]. Materials Science and Engineering A, 2013, 560: 824−830.

[31] TONG L B, CHU J H, JIANG Z H, KAMADO S, ZHENG M Y. Ultra-fine grained Mg−Zn−Ca−Mn alloy with simultaneously improved strength and ductility processed by equal channel angular pressing [J]. Journal of Alloys and Compounds, 2019, 785: 410−421.

[32] WANG B N, WANG F, WANG Z, ZHOU L, LIU Z, MAO P L. Microstructure and mechanical properties of Mg−Zn−Ca−Zr alloy fabricated by hot extrusion-shearing process [J]. Materials Science and Engineering A, 2020, 795: 139937.

[33] YAN Z F, WANG D H, HE X L, WANG W X, ZHANG H X, DONG P, LI C H, LI Y L, ZJOU J, ZHANG L, SUN L Y. Deformation behaviors and cyclic strength assessment of AZ31B magnesium alloy based on steady ratcheting effect [J]. Materials Science and Engineering A, 2018, 723: 212−220.

[34] DAI S, WANG F, WANG Z, LIU Z, MAO P L. Effect of Cu on microstructure, mechanical properties, and texture evolution of ZK60 alloy fabricated by hot extrusion shearing process [J]. Transactions of Nonferrous Metals Society of China, 2020, 30: 1511−1523.

[35] YAMAGUCHI D, HORITA Z, NEMOTO M, LANGDON T G. Significance of adiabatic heating in equal-channel angular pressing [J]. Scripta Materialia, 1999, 41: 791−796.

[36] LV B J, PENG J, PENG Y, TANG A T, PAN F S. Mechanical properties and energy absorption of extruded Mg−2.0Zn−0.3Zr alloy with Y addition [J]. Rare Metals, 2013, 34: 314−323.

[37] HOMMA T, MENDIS C L, HONO K, KAMADO S. Effect of Zr addition on the mechanical properties of as-extruded Mg−Zn−Ca−Zr alloys [J]. Materials Science and Engineering A, 2010, 527: 2356−2362.

[38] ZENGIN H, TUREN Y. Effect of La content and extrusion temperature on microstructure, texture and mechanical properties of Mg−Zn−Zr magnesium alloy [J]. Materials Chemistry and Physics, 2018, 214: 421−430.

[39] PARK S H, YU H, KIM H S, BAE J H, YM C D, YOU B S. Effect of Cu addition on the microstructure and mechanical properties of an as-extruded ZK60 alloy [J]. Korean Journal of Metals and Materials, 2013, 51: 169−179.

[40] JIANG H S, QIAO X G, ZHENG M Y, WU K, XU C, KAMADO S. The partial substitution of Y with Gd on microstructures and mechanical properties of as-cast and as-extruded Mg−10Zn−6Y−0.5Zr alloy [J]. Materials Characterization, 2018, 135: 96−103.

采用挤压剪切工艺制备细晶高强韧镁合金

王柏宁[1,2]，王 峰[1,2]，王 志[1,2]，刘 正[1,2]，毛萍莉[1,2]

1. 沈阳工业大学 材料科学与工程学院，沈阳 110870；
2. 辽宁省镁合金及成形技术重点实验室，沈阳 110870

摘 要：设计一种新型挤压剪切(ES)复合工艺以制备细晶高强韧镁合金。利用有限元软件 Deform-3D，通过正交模拟实验对 ES 模具的结构参数进行优化，并采用 ES 模具对 Mg−3Zn−0.6Ca−0.6Zr(ZXK310)合金进行成形。结果表明，优化的 ES 模具结构参数为挤压角 a=90°、挤压段高度 h=15 mm 以及内圆角半径 r=10 mm。在挤压温度和模具温度为 350 °C 进行挤压剪切时，ZXK310 合金表现出良好的 ES 成形性，且成形区发生明显的动态再结晶，晶粒尺寸从挤压区的 1.42 μm 降低到成形区的 0.85 μm。由于第二相钉扎及超细晶的形成，合金的抗拉强度、屈服强度和伸长率分别达到 362 MPa、289 MPa 和 21.7%。

关键词：Mg−Zn−Ca−Zr 合金；挤压剪切工艺；模具设计；动态再结晶；力学性能

(Edited by Bing YANG)